Ion implantation in tetrahedral amorphous carbon

D. G. McCulloch
Electron Microscope Unit, University of Sydney, New South Wales, 2006, Australia

E. G. Gerstner and D. R. McKenzie
School of Physics, University of Sydney, New South Wales, 2006, Australia

S. Prawer
School of Physics, University of Melbourne, Victoria 3052, Australia

R. Kalish
Solid State Institute and Physics Department, Technion Israel Institute of Technology, Haifa, Israel
(Received 5 December 1994)

Tetrahedral amorphous carbon (*ta*-C) is a dense form of amorphous carbon with a structure consisting of a highly tetrahedral bonding network. Approximately 20% of the atoms in *ta*-C are sp^2 hybridized and the presence of these sites plays an important role in the electrical and optical properties of the material. In the present investigation, we use 50 keV C^+ and 200 keV Xe^+ ion implantation to damage the structure in a controlled manner. The structure of the *ta*-C following ion irradiation is monitored using the dose dependence of the electrical conductivity, Raman spectroscopy, electron diffraction, and electron energy-loss spectroscopy. It is shown that the damage is predominantly reflected in an increased concentration of sp^2-bonded sites. With increasing dose, the structure is observed to change from an essentially tetrahedral network containing sp^2 sites as "defects" to an essentially sp^2-bonded structure in which there is a high degree of in-plane disorder combined with a regular stacking of the planes.

I. INTRODUCTION

It is well established that a dense form of amorphous carbon can be produced by condensation of carbon ions from a filtered vacuum cathodic arc onto various substrates.[1,2] The material has a density of approximately 2.90 g/cc and a structure which has been described as a highly tetrahedral network.[2,3] We will refer to this material as tetrahedral amorphous carbon (*ta*-C). Approximately 20% of the atoms in *ta*-C are sp^2 hybridized with a threefold symmetry with the remainder being sp^3 hybridized with a tetrahedral bonding arrangement.[4] *Ta*-C has the electronic properties of a wide band-gap amorphous semiconductor and is able to accept *n*-type dopants.[5] It also shows photoconductivity[6] and has been used to make rectifying junctions.[7] The band gap is approximately 2.5 eV (Ref. 8) and is considerably smaller than that of diamond. The 20% of sp^2 sites are therefore considered to play an important role in providing a significant density of states inside the wider band gap of the sp^3-bonded structure. These sp^2-derived states may provide the conduction states in the material.

In this paper we use high-energy ion implantation to damage the structure of *ta*-C and to study the effects of this damage on the electrical and optical properties of *ta*-C. We show that this damage is predominantly reflected in an increased concentration of sp^2-bonded sites. Two incident ion species, C^+ and Xe^+ are used in this study in order to provide information on the way in which the damage scales with the mass of the bombarding species. At high sp^2 concentrations, the nature of the network is radically altered and the structural changes which take place are studied using Raman spectroscopy, electron diffraction, and electron energy-loss techniques.

The study of ion damage effects in *ta*-C provides the groundwork for the possible use of ion implantation to dope this material. An understanding of the effects of ion-beam damage on the electrical behavior of *ta*-C is an essential prerequisite for such doping studies. In addition, this investigation provides some preliminary data on the expected radiation hardness of devices fabricated from *ta*-C.

Another motivation for this study is the recent finding that diamond, when bombarded with high-energy ions at or below room temperature, transforms into an amorphous sp^3-bonded state at a critical ion does (D_c).[9,10] This transformation is believed to be analogous to the formation of *a*-Si in response to the ion implantation of crystalline Si. The amorphous sp^3 structure formed in ion implanted diamond is thought to be similar in its properties and microstructure to *ta*-C. In the case of diamond, if the ion dose is increased beyond D_c, the sp^3 bonds in the amorphous structure gradually transform into sp^2 bonds with a concomitant rise in the measured electrical conductivity. Below D_c, thermal or laser annealing can remove most of the radiation damage, with the undamaged diamond acting as a template for the recrystallization of the damaged material.[11,12] In diamond, it is thought that the conversion from sp^3- to sp^2-bonded C is inhibited until the damaged layer amorphizes[9,10,13] and hence no increase in the conductivity is observed until the dose exceeds D_c. The reason for this may be that a

0163-1829/95/52(2)/850(8)/$06.00

large decrease in density accompanies the sp^3 to sp^2 bond conversion and that prior to amorphization, the diamond lattice is rigid enough to prevent bond conversion from occurring. By contrast, for *ta*-C, no crystalline template exists, and hence there is nothing to inhibit the sp^3 to sp^2 bond conversion, and there is no reason to expect a critical dose D_c at which a sharp increase in the electrical conductivity should start to be observed. Hence one would expect the electrical conductivity to rise for much lower doses than the typical values for D_c observed in diamond. In this work we experimentally test these expectations.

II. EXPERIMENTAL

A. Sample preparation

A film of *ta*-C of approximate thickness 20 nm was prepared on a substrate of fused silica using a filtered cathodic arc deposition system of a type discussed previously.[1] The graphite source material was Ringsdorff graphite of purity 99.995%. The film was prepared at room temperature without electrical bias of the substrate holder, so that growth took place from ions of approximately 22 eV energy.[14]

B. Ion implantation and *in situ* resistance measurements

The electrical resistance was measured *in situ* during ion implantation for both 200 keV Xe^+ and 50 keV C^+ ions on specimens provided with electrical contacts consisting of two thick silver strips separated by 0.5 mm.[15] The two point electrical resistance was monitored during implantation. The dose range was 10^{12} to 2.5×10^{15} ions/cm^2 for Xe^+ ions and 10^{12} to 10^{16} ions/cm^2 for C^+. As will be shown below from the comparison of the dose dependence of resistance for Xe and C implants, the dominant factor controlling the transformation is the energy deposited in direct knockon collisions in the collision cascade. Hence, for additional *ex situ* structural studies it was not necessary to investigate both Xe and C implanted samples and only Xe implanted samples were subjected to optical, electrical and electron-diffraction studies. The doses of these Xe implanted specimens are shown in Table I. All specimens were implanted in a DANFYSIK ion implantation system in a vacuum below 10^{-5} Torr. Beam currents on the samples were limited to 1 mA/cm^2 to minimize beam heating during irradiation. The implantation temperature was 493 K. This elevated substrate temperature was chosen because the base line conductivity of the *ta*-C was higher, allowing the measurements to be accomplished more easily.

TABLE I. Properties *ta*-C films implanted with 200 keV Xe^+ ions at 470 K.

Ion dose (cm^{-2})	Carrier	Optical gap, E_g (eV)	Plasmon energy (eV)	sp^2 fraction (%)
0	*p*-type (Ref. 22)	2.5 (Ref. 8)	30.5	26
1×10^{13}		2.3	29.9	27
2×10^{13}	*n*-type	2.1	29.6	31
1×10^{14}	*n*-type	1.6	27.5	46
2×10^{14}	*n*-type	1.2	26.7	48
1×10^{15}	*n*-type	0.7	24.8	82

Both the 200 keV Xe^+ and 50 keV C^+ ions have predicted ranges much greater than the thickness of the *ta*-C film.[16] The effect of Xe implantation on the electrical and optical properties of fused silica has been shown to be negligible[17] and therefore changes in the structural, electrical and optical properties of the *ta*-C films following ion bombardment are primarily due to ion beam damage of the *ta*-C films and not changes in the properties of the silica substrates.

C. Optical measurements

The transmittance T of the specimens was measured over the wavelength range 180 to 700 nm. The absorption coefficient α was calculated by neglecting reflectance losses and using the formula

$$\alpha=-\frac{1}{x}\ln(T)\ , \tag{1}$$

where x is the thickness of the film.

Raman spectra were acquired in a Dilor XY micro-Raman spectrometer using the Ar line at 488 nm, a laser power of 30 mW and a 2 mm spot size. No evidence of laser beam damage was found in any of the specimens. Raman shifts over the range 1000–1800 cm^{-1} were collected with a resolution of 5 cm^{-1}. The absorption coefficient a is sufficiently small at a wavelength of 488 nm that the laser probes the entire thickness of the *ta*-C film.

D. Electron energy-loss spectroscopy

Electron energy-loss spectra were acquired at a resolution of 1.3 eV using a GATAN 666 parallel electron energy-loss spectrometer attached to a Philips EM430 electron microscope operating at 200 keV. Specimens were prepared by dissolving the fused silica substrate in 70% HF and mounting the unsupported films on electron microscope grids. The low loss region up to 100 eV was used to determine the plasmon energy, while the region in the vicinity of the *K*-shell core loss feature at 285 eV was used to determine the fraction of sp^2-bonded carbon. Electron-beam bombardment at 200 keV is not expected to result in detectable damage to *ta*-C since it has been shown that high dose 300 keV exposure produces only a small change in plasmon energy.[18]

E. Electron diffraction

In order to provide further information on the structural changes which occur in *ta*-C following ion implantation, energy filtered electron diffraction data were collected at 300 keV using the techniques described by Cockayne, McKenzie, and Muller.[19] Diffracted intensity was collected in the region around the unscattered beam to a sufficiently large scattering angle to include the position of the graphite {110} reflections.

III. RESULTS

A. Electrical resistivity

Figure 1 shows the dose dependence of the resistivity measured *in situ* during ion implantation for both Xe^+ and C^+ ions. The resistivity decreases even for the lowest doses employed and shows a steady decrease from the initial value followed by a very rapid decrease and then finally, the resistivity saturates to a highly conducting state. The form of the curve is the same for both implanting species. If the carbon dose is rescaled by a factor of approximately 18, the curves overlay closely as shown in Fig. 1. TRIM calculations[16] predict that the ratio of the nuclear stopping powers in *ta*-C for 200 keV Xe^+ and 50 keV C^+ ions is 30:1. The corresponding ratio for electronic stopping powers is 5:1. Thus a ratio of 18 suggests that displacements following nuclear collisions form the most significant part of the damage in implanted *ta*-C.

The temperature dependence of the resistivity was measured *ex situ* using a linear four-point probe arrangement in a helium cryostat. This was performed on an undamaged specimen and the four highest Xe^+ dosed samples as shown in Fig. 2. There are three principal methods of interpreting the temperature dependence of the conductivity of amorphous semiconductors. These are (a) activated conduction via extended states in the conduction band, (b) nearest-neighbor hopping between localized states, and (c) variable-range hopping between localized states. Activated conduction and nearest-neighbor hopping gives rise to a exponential T^{-1} dependence, while variable range hopping has an exponential $T^{-1/4}$ dependence.[20,21] The experimental data shown in Fig. 2 is not well described by either of the above temperature dependencies over the entire temperature range measured. The general trend apparent in Fig. 2 is towards a weak temperature dependence as the implantation dose and electrical conductivity increase. This indicates a change from semiconductorlike behavior at low doses to a metalliclike conduction at high doses, consistent with the formation of a sp^2-bonded layered structure in the high dose material.

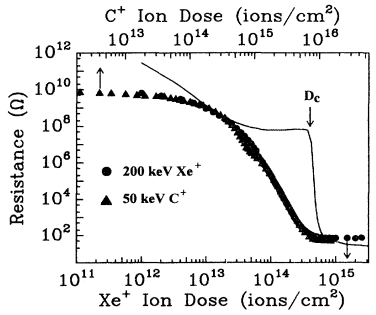

FIG. 1. The dose dependence of the electrical resistance of *ta*-C measured *in situ* during (▲) 50 keV C^+ (top axis) and (●) 200 keV Xe^+ (bottom axis) implantation at 470 K. Also shown for comparison is the dose dependence of the electrical resistance for crystalline diamond implanted with 320 keV Xe^+ ions at 470 K (solid line) (Ref. 10).

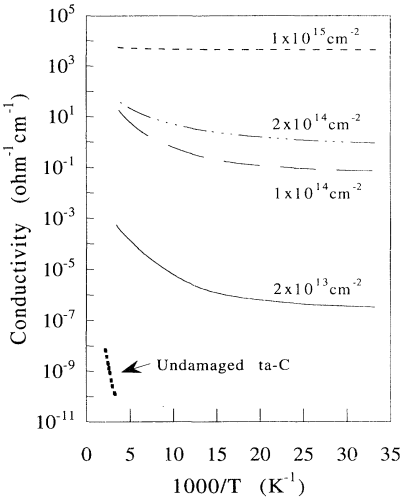

FIG. 2. The resistivity of *ta*-C implanted with various doses of 200 keV Xe^+ ions as a function of reciprocal temperature in Kelvin.

The carrier type of the four highest dose samples was measured using the Seebeck ("hot point") technique. It has been shown that the carrier type in as-grown *ta*-C is *p*-type.[22] It was found that after 200 keV Xe implantation of *ta*-C at doses above 1×10^{13} ion/cm^2, the carrier type changes to *n*-type. The carrier type in diamond irradiated at temperatures of 470 K has also been shown to be *n*-type believed to result from the presence of agglomerated defects contributing to the conductivity.[13] A similar process may be occurring in ion implanted *ta*-C.

B. Optical measurements

The optical gap of an amorphous semiconductor may be found from the wavelength dependence of the absorption coefficient. We determined the absorption coefficient $\alpha(\omega)$ from transmittance measurements of the samples as a function of photon energy and used the relation

$$\hbar\omega\alpha(\omega)=\text{const}(\hbar\omega-E_0) \tag{2}$$

to define the optical gap, E_0. Davis and Mott[20] observed that this relation applies to materials in which "chains or planes of strongly bonded atoms are present." The linear relation for $\hbar\omega\alpha$ in Eq. (2) applies to a limited range above the Urbach edge which shows an exponential dependence. We fitted this linear region to obtain an estimate for the optical gap, E_0. Figure 3 shows plots of $\hbar\omega\alpha(\omega)$ as a function of photon energy for five of the Xe implanted specimens. The optical gap E_0 is plotted as a function of dose in Fig. 4 and shows a general decrease with dose, with a large decrease at doses in the dose region around 10^{14} cm^{-2}.

The Raman intensity is shown in Fig. 5 for all specimens including, for comparison, a sample of glassy car-

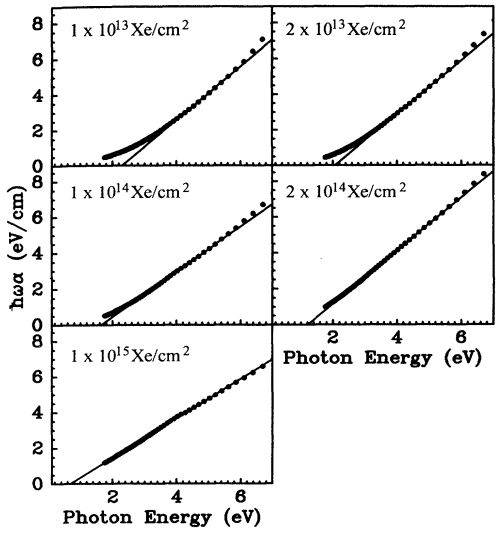

FIG. 3. Quantity $\hbar\omega\alpha$ is plotted against photon energy $\hbar\omega$ for the *ta*-C specimens implanted to the doses shown in Table I. The horizontal intercept of the straight line fitted above the Urbach edge approximates the optical gap.

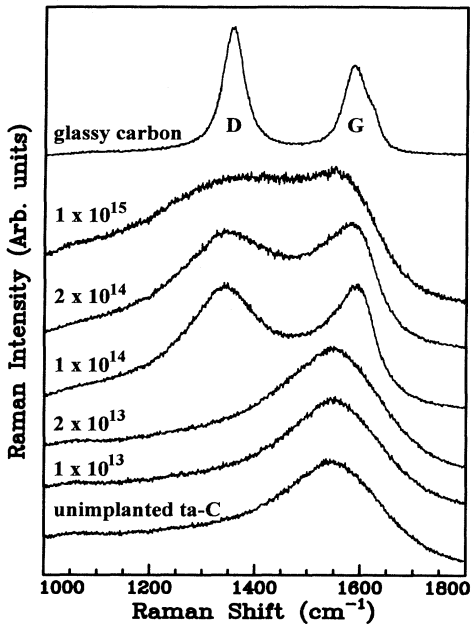

FIG. 5. The effect of 200 keV Xe ion implantation on the Raman spectrum of *ta*-C implanted to the doses shown. Also shown for comparison is the Raman spectrum glassy carbon. The *G* and *D* refer to the graphite and disorder peaks, respectively.

bon (heat treated at 2500 °C). The unimplanted *ta*-C shows a single asymmetrical peak with a maximum lying between the *D* (disorder peak) and *G* (graphite peak) peaks of glassy carbon. The Raman spectra reflect the single phonon vibrational density of states since the *k*-selection rules do not apply in these amorphous structures. The *G* peak also occurs in crystalline graphite while the *D* peak occurs in many disordered graphitic materials. The peak in unimplanted *ta*-C is similar to that observed in other amorphous carbons.[23] The lower position of this peak relative to the *G* peak in glassy carbon has been ascribed either to a bond angle disorder in sheetlike sp^2-bonded carbons or to the presence of some tetrahedral bonding.[24] It is important to stress that the Raman spectrum is predominantly sensitive to in-plane modes in sp^2-bonded materials and in particular the scattering above approximately 1400 cm^{-1} cannot be due to sp^3-bonded material according to density of states calculations.[25] Therefore the Raman spectrum provides information on the bonding within the sp^2 fraction of the *ta*-C film.

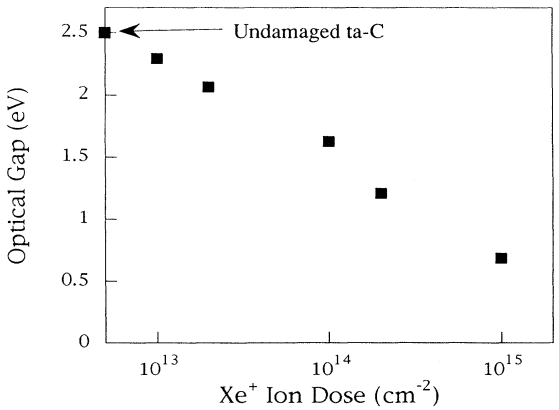

FIG. 4. The optical gap plotted as a function of ion dose for *ta*-C implanted with 200 keV Xe^+ to the doses shown.

A sudden qualitative change in the Raman spectrum appears at a dose of 10^{14} ions/cm^2: a pronounced *D* peak emerges concurrent with the development of a *G* peak. The *D* peak corresponds to a feature in the vibrational density of states of layered sp^2 structures such as graphite.[26] The *G* peak corresponds to the zone center E_{2g} Raman active mode of graphite.[26] These spectra therefore imply that a structural change occurs at a dose of 10^{14} ions/cm^2 from a highly disordered material to one which contains a significant fraction of sp^2-bonded material with good in-plane ordering.

At higher doses than 10^{14} ions/cm^2, both the *D* and *G* peaks become broadened and less well defined. A phenomenon similar to this has already been observed in implanted graphite[27] and glassy carbon,[28] where it has been attributed to increasing in-plane disorder within the graphite layers.

C. Electron energy-loss spectroscopy

Energy-loss spectra of carbon films in the vicinity of the *K* edge are useful indicators of the density of states of

unoccupied electron levels. The feature labeled π^* in Fig. 6 is characteristic of the states arising from sp^2 bonds and can be used to quantify the fraction of sp^2 bonded carbon atoms by integrating its intensity relative to the main core loss feature. The spectra of Fig. 6 show the progressive evolution of the π^* feature with increasing dose culminating in a spectrum similar to that of the glassy carbon (also shown). The additional structure in the glassy carbon K edge around 300 and 330 eV can be attributed to the presence of long-range spacial correlations resulting from the presence of graphitelike ribbons in glassy carbon. The fraction of sp^2 bonds in the ion implanted *ta*-C specimens was calculated[4] from

$$f=\frac{sp^2}{sp^2+sp^3}=\frac{I_{u\pi^*}}{I_{g\pi^*}}\frac{I_g(\Delta E)}{I_u(\Delta E)}\ , \tag{3}$$

where $I_{u\pi^*}$ is the integral under the π^* feature of the sample, while $I_u(\Delta E)$ is the integral under the edge as a whole over an interval ΔE. $I_{u\pi^*}$ was calculated after removing overlap with the main core loss feature by linear extrapolation of the leading edge to this principal peak. $I_{g\pi^*}$ and $I_g(\Delta E)$ are the corresponding quantities for a 100% sp^2-bonded carbon. Since the intensity of the 1*s* to π^* peak from single-crystal graphite depends on the beam-to-crystal orientation,[4] $I_{g\pi^*}$ was measured from glassy carbon which has an isotropic sp^2-bonded structure. Figure 7 shows the results for f as a function of dose. The first four points show a linear dependence of f on the dose, which is expected for small doses since damage tracks will rarely overlap. At a dose of 10^{14} ion/cm^2, f has become less sensitive to further dose, the material now being more stable and therefore less sensitive to ion-beam damage.

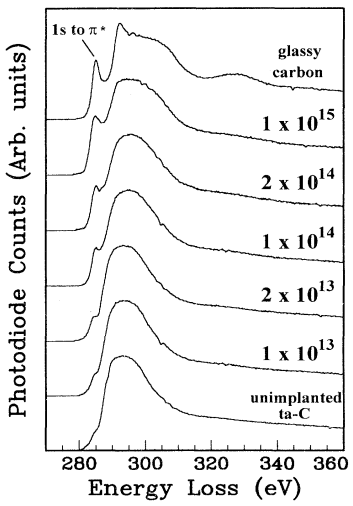

FIG. 6. Background-subtracted electron-energy-loss spectra in the carbon *k*-edge region for the *ta*-C specimens implanted to the doses. The characteristic feature resulting from the 1*s* to π^* transitions is shown.

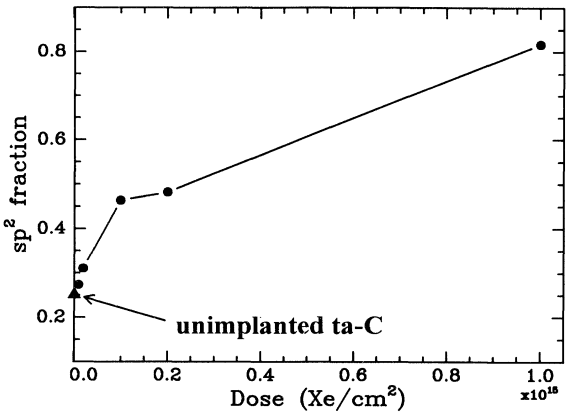

FIG. 7. The fraction of sp^2 bonds in the *ta*-C specimens calculated from Eq. (3) as a function of the Xe ion doses shown in Table I.

The plasmon energy was determined for each specimen from the low loss region of the energy-loss spectrum. The plasmon energy may be related to the volume density of electrons taking part in volume excitations, and hence to the physical density if a constant four valence electrons per atom is assumed. The relation between the plasmon energy E_p and the volume density of conduction electrons N is,[29]

$$E_p^2=\frac{Ne^2}{\varepsilon_0 m}\ . \tag{4}$$

The plasmon energy and the derived density are shown in Fig. 8. After the disappearance of the tetrahedral network at 10^{14} ions/cm^2, the plasmon energy is more resistant to further change.

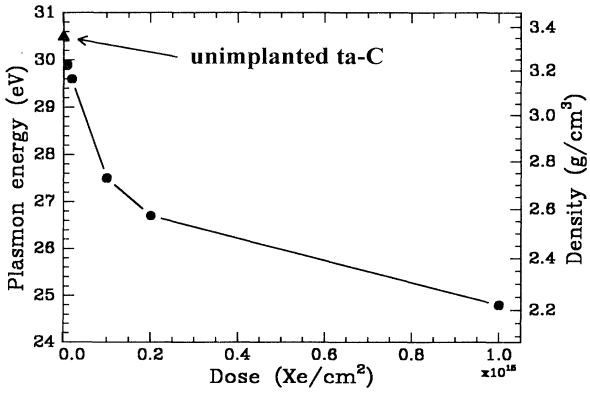

FIG. 8. The plasmon energy of the *ta*-C specimens as a function of the Xe doses shown in Table I. The right-hand axis shows the density which corresponds to each plasmon energy calculated from Eq. (4).

D. Electron diffraction

Electron diffraction provides further insights into the structural changes discussed above. The region around the undiffracted beam contains information on the longer-range spatial correlations in the specimen. Figure 9 shows the energy filtered elastic electron-diffraction intensity for all specimens and for glassy carbon. The diffraction pattern for *ta*-C has been described in the literature[30] and contains very little intensity near the undiffracted beam, indicating a homogeneous network without inhomogenities on a scale larger than about 0.35 nm. Beam damage up to a dose of 2×10^{14} ions/cm^2 produces a general enhancement of scattering near the central beam indicating inhomogenities over a large range of sizes. This increase in small angle scattering can probably be attributed to cracks or void spaces resulting from damage. At a dose of 1×10^{15} ions/cm^2 the small-angle scattering again decreases indicating an increase in homogeneity.

Also evident in Fig. 9 is the formation of a peak in the position of the graphite {002} reflections for a dose of 10^{14} ions/cm^2. The emergence of {002} reflections indicates the presence of layers separated by the distance between layers in graphite (0.334 nm). This peak continues to increase in intensity and decrease in breadth, indicating an increasing tendency towards larger and more perfectly spaced layers. The in-plane ordering, however, of the graphitelike layers as indicated by the intensity of the peaks at the graphite {100} and {110} positions, reaches a maximum at 10^{14} ions/cm^2 but decreases with further dose, in agreement with the Raman observations. This interpretation is made by comparing the diffraction patterns of the specimens with that of glassy carbon which gives the expected relative intensity of the {002} and the {100} and {110} reflections for well ordered graphitelike layers containing six-membered rings.[31]

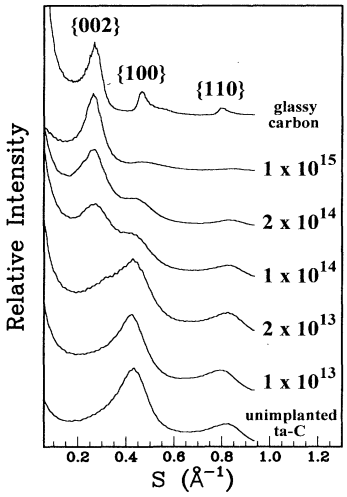

FIG. 9. Energy filtered electron-diffraction intensities from the *ta*-C specimens implanted with 200 keV Xe^+ ions to the doses shown. Also shown for comparison, is the diffraction pattern from glassy carbon.

IV. DISCUSSION

The dose dependence of the conductivity of ion-irradiated *ta*-C shown in Fig. 1 is different to that shown by other forms of carbon including hydrogenated amorphous carbon,[15] type-II natural diamond,[32] CVD diamond,[32] and C_{60} fullerene,[33] which all show a well-defined threshold dose before the resistivity begins to decrease. For the specific case of diamond irradiated with 320 keV Xe^+ at 490 K there is a transition at a critical dose, D_c (see Fig. 1 which compares the data for *ta*-C to that of natural diamond). For doses $<D_c$ the gradual increase in conductivity is believed to be due to hopping conductivity between islands of highly conducting graphitelike material.[11,12] At D_c these islands overlap to form a continuous electrical pathway through the irradiated volume leading to a very rapid decrease in the resistance. For *ta*-C this clearly does not occur; there is no critical dose where a sudden decrease in resistance is observed, or a dose where a sudden change in the band gap or activation energies occurs. This suggests that the origin of the conductivity in ion implanted *ta*-C is different to that in ion implanted diamond. We offer the following tentative explanation.

Unirradiated *ta*-C contains sp^2 sites at a concentration of about 20% and these sites form midgap impurity states. Density of electronic states calculations of model structures by a number of authors[26,34] show a decreasing gap with increasing sp^2 fraction. We suppose that the passage of each ion creates further sp^2-bonded material, which can contribute to the conductivity by acting as *n*-type dopants. The presence of a greater proportion of sp^2-bonded material also narrows the gap between the conduction or valance mobility edges which leads to a gradual increase in the conductivity and the decrease in the optical gap.

The sudden structural transformations observed by electron diffraction and Raman spectroscopy which occur at a Xe dose of about 10^{14} ions/cm^2 are not accompanied by sharp changes in the electrical behavior. A possible explanation for this may be as follows. As the dose is increased, the probability of sp^2 sites clustering into isolated graphitic islands increases. As long as these sp^2 clusters are isolated from each other, they will not contribute significantly to the conductivity (or rather their contribution will be small as compared to that from the sp^2 sites within the sp^3 matrix). The Raman and TEM measurements are sensitive to the ordering within these graphitic islands, and it is clear that this ordering increases dramatically at a dose of about 10^{14} ions/cm^2. When the sp^2-bonded zones overlap, the conductivity is expected to saturate and indeed this does occur at a dose of about 10^{15} ions/cm^2. These results suggest that the electrical properties of the virgin material are primarily due to the presence of defect states caused by local deviations from sp^3 bonding.

As discussed above, Raman spectroscopy and electron diffraction are sensitive to different aspects of the implanted *ta*-C structure. Raman spectroscopy is primarily sensitive to the in-plane order of the sp^2 fraction of the irradiated *ta*-C, whereas the electron diffraction provides

information on the entire (three-dimensional) structure. In order to assist the reader in understanding the structural changes which occur during the ion implantation of *ta*-C, Fig. 10 shows a schematic impression of "snapshots" in the evolution of the amorphous tetrahedral structure when viewed from two directions perpendicular to one another (plan view and side view). The unimplanted *ta*-C (represented by dark grey in the figure) is isotropic and contains a majority of fourfold-coordinated sp^3-bonded sites. As ion implantation proceeds, the ion produces damage in the form sp^2-bonded carbon atoms and at a dose of approximately 10^{14} Xe/cm^2 the structure consists of a considerable fraction of sp^2-bonded carbon (approximately 50%) in the form of isolated graphitic regions (six-membered rings, white in the diagram) surrounded by undamaged *ta*-C material. As shown in the plan view of Fig. 10(b), these isolated islands form sp^2-rich nuclei and have a considerable degree of in-plane order, that is, a predominance of hexagonal six membered rings as indicated by the Raman analysis. The broad {002} reflection in the diffraction pattern at this dose indicates, however, that the *c*-axis stacking of these nuclei is poor as shown in the right-hand side of Fig. 10(b). As the implantation continues to doses above 10^{14} Xe/cm^2, and the sp^2 fraction increases, the in-plane bonding becomes increasingly disordered as indicated by a broadening of the Raman peaks. This implies that, in the implanted *ta*-C sheet structures, a variety of ring sizes, that is, many five- and seven-membered rings are present [light grey in Fig. 10(c)] along with six-membered rings. At the same time, the stacking of the sp^2-bonded regions becomes increasingly ordered, as indicated by a narrowing of the {002} reflection in the diffraction pattern. Figure 10(c) illustrates this microstructure at a dose of about 10^{15} ions/cm^2 where the structure has become almost entirely sp^2 bonded. Large regions of conducting material have been formed, as indicated by a dose saturation of the resistance at a low value. The conduction mechanism at this dose is essentially metallic as in graphite.

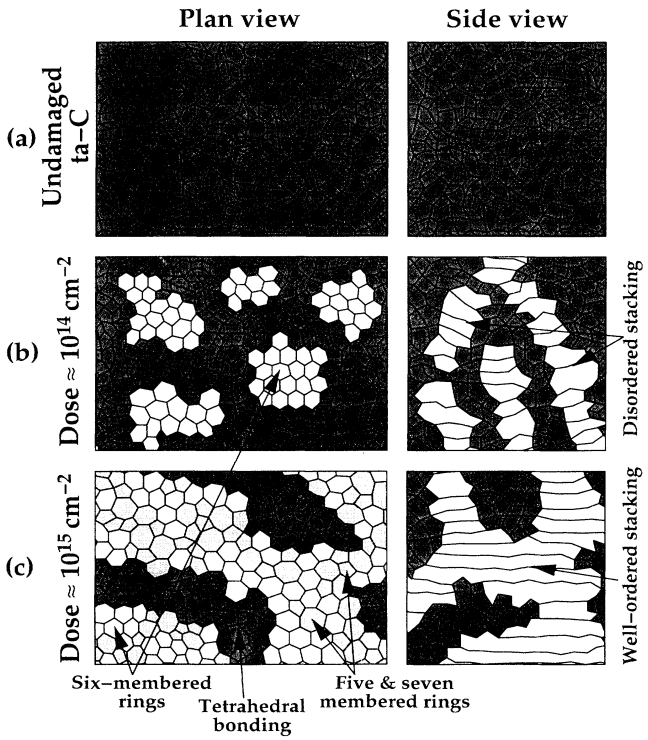

FIG. 10. Sketches to illustrate the evolution of the *ta*-C into a disordered sp^2 structure with increasing Xe ion dose when viewed from two directions perpendicular to one another. (a) illustrates the structure of virgin *ta*-C, while (b) and (c) show the structure following 200 keV Xe implantation at 470 K to doses of approximately 10^{14} ions/cm^2 and 10^{15} ions/cm^2, respectively. The dark grey regions are undamaged *ta*-C, the white regions represent graphitelike six-membered rings, while light grey represents regions containing five- and seven-membered rings.

The appearance and subsequent disappearance of in-plane order within the implanted *ta*-C structure requires some discussion. It has been shown that C interstitials are mobile for implantation temperatures of 500 K in ion implanted glassy carbon, and that above this temperature, defect mobilities are sufficient so that the glassy carbon structure is retained even after high ion doses.[35] Therefore for an implantation temperature of 470 K, defect mobilities in the ion-beam-modified *ta*-C are probably sufficiently high to allow knockon carbon atoms generated in the collision cascade to reorganize into islands of sp^2-bonded carbon with a considerable degree of in-plane order [see Fig. 10(b)]. At even higher doses, the size of these sp^2-bonded regions increases, but on the other hand the ion beam introduces considerable damage, so that the in-plane order is degraded [see Fig. 10(c)].

V. CONCLUSIONS

The effect of ion implantation on the structure and electrical behavior of *ta*-C has been investigated. Unlike other insulating forms of carbon, no critical dose for the onset of conductivity was observed. Rather, the resistance and optical band gap decrease as a gradual function of ion dose. By contrast, the Raman and diffraction measurements show a sudden change in structure at a Xe^+ dose of about 10^{14} ions/cm^2 where a high fraction of well-ordered sp^2-bonded carbon atoms in graphitelike nuclei is observed. Further ion bombardment increases the sp^2 fraction, concurrent with a disruption of the in-plane sp^2 order. The resulting material contains a high degree of layerlike stacking with poor in-plane order. Since the addition of sp^2 sites by ion damage has an immediate effect on the conductivity of *ta*-C, the central role of these sites in conduction is confirmed. The results suggest that the conductivity of as grown *ta*-C is dominated by the presence of sp^2 defect sites distributed throughout the network.

The results also show that highly conducting pathways can be "written" into *ta*-C by selecting the appropriate dose and energy using an ion beam. The results therefore give the necessary parameters for the construction of electrical contacts or conducting pathways useful in fabricating possible devices from *ta*-C.

[1]I. I. Aksenov, V. A. Belous, V. G. Padalka, and V. M. Khorosikh, Fiz. Plazmy **4**, 758 (1978) [Sov. J. Plasma Phys. **4**, 425 (1978)].
[2]D. R. McKenzie, D. A. Muller, and B. A. Pailthorpe, Phys. Rev. Lett. **67**, 1286 (1991).
[3]P. H. Gaskell, A. Saeed, P. Chievx, and D. R. McKenzie, Phys. Rev. Lett. **67**, 12 869 (1991).
[4]S. D. Berger, D. R. McKenzie, and P. J. Martin, Philos. Mag. Lett. **57**, 285 (1988).
[5]V. S. Veerasamy, C. A. J. Amaratunga, C. A. Davis, A. E. Timbs, W. I. Milne, and D. R. McKenzie, J. Phys. Condens. Matter **5**, L169 (1993).
[6]G. A. J. Amaratunga, V. S. Veerasamy, W. I. Milne, C. A. Davis, S. R. P. Silva, and H. S. McKenzie, Appl. Phys. Lett. **63**, 370 (1993).
[7]D. R. McKenzie, Y. Yin, N. A. Marks, C. A. Davis, E. Kravtchinskaia, B. A. Pailthorpe, and G. A. J. Amaratunga, J. Non-Cryst. Solids **164-166**, 1101 (1993).
[8]P. D. Swift, Ph.D. thesis, University of Sydney, 1986.
[9]A. Hoffman, S. Prawer, and R. Kalish, Phys. Rev. B **45**, 12 736 (1992).
[10]S. Prawer (unpublished).
[11]S. Prawer, D. N. Jamieson, and R. Kalish, Phys. Rev. Lett. **69**, 2991 (1992).
[12]R. Kalish, Diam. Relat. Mater. **2**, 621 (1993).
[13]C. Uzan-Suguy, V. Richter, S. Prawer, Y. Lifshitz, E. Grossman, and R. Kalish, Diam. Relat. Mater. (to be published).
[14]P. J. Martin, S. W. Filipczuk, R. P. Neterfield, J. S. Field, D. F. Whitnall, and D. R. McKenzie, J. Mater. Sci. Lett. **7**, 410 (1988).
[15]S. Prawer, R. Kalish, M. Adel, and V. Richter, J. Appl. Phys. **61**, 4492 (1987).
[16]J. F. Ziegler, J. P. Biersack, and U. Littmark, *The Stopping and Range of Ions in Solids* (Pergamon, New York, 1985).
[17]S. Prawer, A. Hoffman, M. Petravic, and R. Kalish, J. Appl. Phys. **73**, 3841 (1993).
[18]C. A. Davis, D. R. McKenzie, Y. Yin, E. Kravtchinskaia, G. A. J. Amaratunga, and V. S. Veerasamy, Philos. Mag. B **69**, 1133 (1994).
[19]D. J. H. Cockayne, D. R. McKenzie, and D. A. Muller, Microsc. Microanal. Microstruct. **2**, 359 (1991).
[20]E. A. Davis and N. F. Mott, Philos. Mag. **22**, 903 (1970).
[21]N. F. Mott, *Conduction in Non-Crystalline Materials,* 2nd ed. (Clarendon, Oxford, 1993).
[22]G. A. J. Amaratunga, D. E. Segal, and D. R. McKenzie, Appl. Phys. Lett. **59**, 69 (1991).
[23]R. O. Dillon, J. A. Woollam, and V. Katkanant, Phys. Rev. B **29**, 3482 (1984).
[24]D. Beeman, J. Silverman, R. Lynds, and M. R. Anderson, Phys. Rev. B **30**, 870 (1984).
[25]C. Z. Wang and K. Ho, Phys. Rev. Lett. **71**, 1184 (1993).
[26]R. Al-Jishi and G. Dresselhaus, Phys. Rev. B **26**, 4514 (1982).
[27]B. S. Elman, M. S. Dresselhaus, G. Dresselhaus, E. W. Maly, and H. Mazurek, Phys. Rev. B **24**, 1027 (1981).
[28]D. G. McCulloch, S. Prawer, and A. Hoffman, Phys. Rev. B **50**, 5905 (1994).
[29]R. F. Egerton, *Electron Energy Loss Spectroscopy in the Electron Microscope* (Plenum, New York, 1986).
[30]D. R. McKenzie, P. J. Martin, S. B. White, Z. Liu, W. G. Sainty, D. J. H. Cockayne, and D. M. Dwarte, Les Editions de Physique **17**, 203 (1987).
[31]S. Prawer and C. J. Rossouw, J. Appl. Phys. **63**, 4435 (1988).
[32]S. Prawer, A. Hoffman, and R. Kalish, Appl. Phys. Lett. **57**, 2187 (1990).
[33]R. Kalish, A. Samoiloff, A. Hoffman, C. Uzan-Saguy, S. Prawer, and D. McCulloch, Phys. Rev. B **48**, 18 235 (1993).
[34]U. Stephan, T. Frauenheim, P. Blaudeck, and G. Jungnickel, Phys. Rev. B **50**, 1489 (1994).
[35]D. G. McCulloch and S. Prawer, J. Appl. Phys. (to be published).

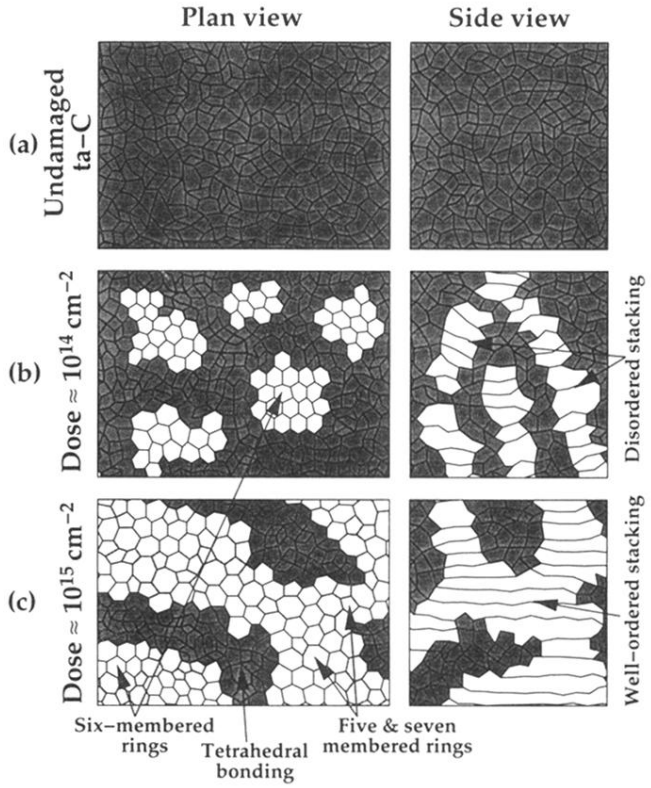

FIG. 10. Sketches to illustrate the evolution of the *ta*-C into a disordered sp^2 structure with increasing Xe ion dose when viewed from two directions perpendicular to one another. (a) illustrates the structure of virgin *ta*-C, while (b) and (c) show the structure following 200 keV Xe implantation at 470 K to doses of approximately 10^{14} ions/cm^2 and 10^{15} ions/cm^2, respectively. The dark grey regions are undamaged *ta*-C, the white regions represent graphitelike six-membered rings, while light grey represents regions containing five- and seven-membered rings.